

**Supporting Information**

**Controlling Glass Forming Kinetics in 2D Perovskites Using Organic Cation Isomers**

*Akash Singh<sup>1,2,#</sup>, Yi Xie<sup>1,2,#</sup>, Curtis Adams III<sup>2</sup>, Benjamin G. Bobay,<sup>3</sup> David B. Mitzi<sup>\*,1,4</sup>*

<sup>1</sup>Department of Mechanical Engineering and Materials Science, Duke University, Durham, North Carolina 27708, United States

<sup>2</sup>University Program in Materials Science and Engineering, Duke University, Durham, North Carolina 27708, United States

<sup>3</sup>Duke University NMR Center, Duke University Medical Center, Durham, North Carolina 27710, United States

<sup>4</sup>Department of Chemistry, Duke University, Durham, North Carolina 27708, United States

\*Corresponding author: david.mitzi@duke.edu

# These authors contributed equally to this work.

## Methods:

### 1. Materials:

(*S*)-(-)-1-(2-naphthyl)ethylamine (S-(1-2)NEA, >99%, Sigma Aldrich), lead bromide (PbBr<sub>2</sub>, 99.99%, TCI chemicals), hydrobromic acid (HBr) (48 wt% in H<sub>2</sub>O, >99.99%, Sigma Aldrich), methanol (CH<sub>3</sub>OH, Semi Grade, VWR chemicals) were procured and used without further purification.

### 2. Crystal synthesis:

For single crystal x-ray diffraction (SCXRD), conventional and ultrafast differential scanning calorimetry (DSC), and melt processing of thin-films, the (*S*)-(-)-1-(2-naphthyl)ethylammonium lead bromide (S(1-2)NPB) crystals were prepared by the slow evaporation method. 0.125 mmol of molecular amine S(1-2)NEA and 0.125 mmol of PbBr<sub>2</sub> were added in 3 ml of HBr with further addition of 4 ml CH<sub>3</sub>OH to completely dissolve the precursors in a glass vial. The vial containing the prepared solution was sealed with Teflon tape and a few holes were poked to allow evaporation of CH<sub>3</sub>OH. After two weeks of evaporation, transparent and laminar crystals of S(1-2)NPB were obtained, which were then cleaned and filtered using diethyl ether. For thermogravimetric analysis (TGA) and <sup>1</sup>H nuclear magnetic resonance (NMR) measurements, S(1-2)NPB crystals were prepared using the slow cooling method. 1:1 equimolar ratio of PbBr<sub>2</sub> (0.1 mmol) and S(1-2)NEA organic amine (0.1 mmol) were added in 1.6 ml of HBr in a glass vial. The solution was heated to 95 °C to dissolve the precursors and subsequently cooled to 20 °C over 48 hours to obtain S(1-2)NPB crystals.

### 3. Melt processing of films:

Soda-lime glass substrates (25.4 × 10.0 × 1.2 mm<sup>3</sup>) were cleaned using sonification in deionized water, acetone, and isopropyl alcohol, each for three minutes, followed by air drying. A few single crystals (< 1.0 mg) of S(1-2)NPB perovskite were placed on a soda-lime lime glass substrate. Crystals were then covered with a 20 μm-thick Kapton sheet and placed onto a preheated hot plate at 225 °C (30 °C beyond the melting point, in order to reduce viscosity and facilitate spreading); the structure was pressed on top with another preheated soda lime glass substrate to spread the melt. After visual inspection to ensure melting (≈60 s), the overlying glass substrate was removed, and the thin-film melt was left to heat for another 30 s before being quickly placed on a metallic steel bench to rapidly cool to room temperature. To facilitate further crystallization (see Figure 3), the melted film was reheated at 140 °C for 5 minutes.

### 4. Single crystal X-ray diffraction:

While conducting the current study, Moon *et. al.* reported the structure for S(1-2)NPB.<sup>1</sup> We independently determined the structure for this system, and the crystallographic results are entirely consistent with this earlier report. Given that the refinement parameters were slightly better for the current study, and since we used our own structure (Table S1) for the analysis described in the paper, the redetermined S(1-2)NPB structure is provided as Supporting Material.

Single-crystal X-ray diffraction (SC-XRD) characterization was carried out on a Rigaku XtaLAB Synergy-S diffractometer using Mo K $\alpha$  radiation ( $\lambda=0.71073$  Å) and operating at 50 kV and 30 mA at room temperature (298K). Peak hunting, data reduction, and numerical absorption correction for all collected data were performed using CrysAlisPro. The crystal structures were solved and refined using SHELXS direct methods and SHELXL least-squares method within the Olex2 software package.

#### 5. Powder X-ray diffraction:

The X-ray diffraction (XRD) measurements of powdered crystals and thin films were performed on a PANalytical Empyrean Powder X-ray diffractometer using Cu K $\alpha$  radiation, with the X-ray tube operating at 45 kV and 40 mA. Measurements are provided over the  $2\theta$  range of  $3^\circ$  to  $30^\circ$  for the crystallization study (Figure 3 and Figure S2).

#### 6. Conventional calorimetric measurements:

DSC measurements were performed using a TA Discovery DSC 2500 instrument using hermetically sealed aluminum pans and lids. Prior to the experiments, the DSC setup was calibrated with metallic indium (melting temperature ( $T_m$ ):  $156.6$  °C; enthalpy of melting:  $28.71$  J/g) using a  $5^\circ\text{C min}^{-1}$  temperature ramp; repeating the calibration cycle showed an acceptable temperature offset of  $0.2$  °C and melting enthalpy offset of  $0.04$  % for the indium standard. DSC analyses of the crystalline S(1-2)NPB perovskite sample was carried out by first hermetically sealing crystals ( $\sim 4.0$  mg) in an aluminum pan/lid, and then conducting the DSC analyses under nominally non-isothermal conditions. The SNPB-crystals were heated from  $20$  °C to  $250$  °C at a ramp rate of  $5^\circ\text{C/min}$ , which resulted in melting of the crystals, followed by cooling at  $50$  °C/min (maximum achievable cooling rate in a conventional DSC) back to  $20$  °C. For cyclic DSC, the S(1-2)NPB sample ( $\sim 4.0$  mg) was heated at  $10$  °C/min from  $20$  °C to  $210$  °C (to avoid more significant decomposition after melting), followed by cooling at  $50$  °C/min to  $-40$  °C. Two more iterations of heating and cooling between  $-40$  °C and  $210$  °C were carried out at a ramp rate of  $10$  °C/min and  $50$  °C/min, respectively. The melting temperature ( $T_m$ ) was calculated using the intersection between the corresponding DSC peak onset with its horizontal baseline. The enthalpy of crystallization ( $\Delta H_c$ ) and melting ( $\Delta H_m$ ) were calculated by measuring the area under the curve relating heat flow ( $W/g$ )/ramp rate ( $^\circ\text{C/s}$ ) and temperature. The entropy of melting ( $\Delta S_m$ ) is obtained by dividing the  $\Delta H_m$  by  $T_m$  in Kelvin scale.

## 7. Thermogravimetric analysis:

TGA measurements were performed on a TA Q50 instrument using a 5 °C/min ramping rate from 25 to 350 °C under nitrogen gas flow (40 ml/min) with samples (~6 mg) of single crystals of S-(1-2)NPB perovskite. For isothermal TGA measurements, the S(1-2)NPB crystals (~6 mg) were first heated from 25 to 195 °C at 10 °C/min and then held at 195 °C for 22 hours until complete organic loss was anticipated from the observed weight loss.

## 8. Nuclear magnetic resonance:

For <sup>1</sup>H NMR measurements, three types of samples were prepared: i) pristine S(1-2)NPB crystals, ii) crystals that underwent one cycle of melt-quenching, and iii) crystals that underwent three cycles of melt-quenching. To obtain the melt-processed samples (ii and iii), the pristine S(1-2)NPB crystals were placed on a sodalime glass substrate, which was placed on a preheated hotplate maintained at 210°C. Upon visual confirmation of melting (~60 s), the substrate was immediately placed on a copper strip for cooling, and the obtained sample is scratched for NMR measurement. For sample (iii), the same procedure was repeated three times. Notably, in the current melt-processed samples, the melt is not covered or confined by a top superstrate, which is expected to allow for more rapid decomposition relative to the more typical conditions used during melt-processing of films, wherein there a top cover is used (see Section 3 above). <sup>1</sup>H NMR spectra were recorded on a Varian INOVA (800 MHz) spectrometer with a cryogenic probe at room temperature. Samples were approx. 1 mM in concentration, including the pristine S(1-2)NPB crystals and the melt-quenched S(1-2)NPB crystals after one and three thermal cycles, respectively. All data were processed and analyzed using MNova (v 14.2.1) and 1 Hz line broadening. Chemical shifts are reported in ppm from tetramethylsilane (TMS) with the solvent resonance resulting from incomplete deuteration (DMSO:  $\delta$  2.47) as the internal reference.

## 9. Ultrafast calorimetric measurements:

Ultrafast (“flash”) DSC measurement was performed using the flash-DSC1 instrument (with UFS-1 chip-sensor) manufactured by Mettler Toledo. The technical specification of the instrument suggests that cooling rates up to 4,000 °C/s are supported in the temperature range of -100 °C – 450 °C. Programming a higher cooling rate (>4000 °C/s) as the measurement parameter is possible; however, doing so results in loss of information at lower temperatures due to undershoots and the sudden drive to equilibrate at the end temperatures.<sup>2</sup> The UFS-1 chip sensor was mounted into the flash-DSC1 instrument and was conditioned and corrected over the temperature range of -100 °C to 450 °C to release any inbuilt stress. The N<sub>2</sub> flow was maintained at 35 ml/min throughout the series of experiments. After this step, a tiny volume of silicone oil (type 47V, 60000, purchased from Silitech AG and recommended for use in the flash-DSC for temperatures up to 350 °C)<sup>3</sup> was applied to the central active region and a measurement (heat and cool cycle with oil only) was carried out in the temperature range of interest (-95 °C to 210 °C) at 250 °C/s (Figure S3). After the run, as-prepared single crystals of S(1-2)NPB were poured on a glass slide and a small single crystal flake (~166 ng) was isolated under an optical microscope and affixed to the flash-DSC by submerging it (to circumvent the organic and hydrogen bromide loss) in the pre-existing silicone oil on the UFS-1 chip using a hair isolated from a hairbrush.

Preliminary testing: To prospectively observe melting, glass formation, and crystallization phenomenon, 3 iterations of the heat and cool cycle were performed on the sample with the initial parameters set to ramp from room temperature ( $\sim 25$  °C) to 210 °C at 250 °C/s, with subsequent isothermal hold (dwell) of 0.5 second (to facilitate complete melting and thermal contact), before cooling to -95 °C at 250 °C/s. Ramp rate of 250 °C/s was selected to achieve a higher signal-to-noise ratio. Decreasing the ramp rate below this value results in noisy data and could potentially degrade the sample due to prolonged exposure to higher temperatures. After this step, 2 iterations of heating and cooling at 250 °C/s were performed between -95 °C to 210 °C with isothermal hold (dwell) time of 0.1 second at end temperatures, before finally heating to room temperature (25 °C). Due to the very small sample sizes and effective thermal contact between the sample and sensor, very short equilibration times are needed relative to conventional DSC. For instance, the time constant of the UFH-1 sensor is about 0.2 ms, i.e., approximately 5000 times less than that of a conventional DSC instrument.<sup>4</sup>

Study of critical cooling rate: After observing the melting, partial glass formation and cold crystallization phenomenon in the preliminary testing, the critical cooling rate (CCR) was determined (using the signature of glass formation during cooling and cold crystallization during heating) by subjecting the melted sample to different cooling rates. Hence, the instrument was programmed to heat the sample from room temperature to 205 °C at 250 °C/s, with dwell time of 0.05 second, with the following steps. (i). Cool from 205 °C to -95 °C at  $x$  °C/s; (ii). Isothermal hold (dwell) at -95 °C for 0.05 second; (iii). Heat from -95 °C to 205 °C at 250 °C/s; (iv). Isothermal hold (dwell) at 205 °C for 0.05 second. Repeat steps (1) – (4) with  $x = 250, 500, 1000, 2500, 5000,$  and 250 °C/s before heating the sample back to room temperature (25 °C).

Study of crystallization kinetics: For the kinetics study, the instrument was programmed to reach 205 °C from 25 °C at 250 °C/s and isothermally held at 205 °C for 0.05 seconds. After this step, the instrument sequence was appended with the following iterative steps: 1. Cool from 205 °C to -95 °C at 2500 °C/s; 2. Isothermal hold (dwell) at -95 °C for 0.05 second; 3. Heat from -95 °C to 205 °C at  $y$  °C/s; where  $y = 50, 250, 500, 1000, 2500,$  and 5000 °C, respectively; 4. Isothermal hold (dwell) at 205 °C for 0.05 second. Steps (1) – (4) were repeated with different  $y$  values in step (3). To examine if there was any change incurred due to thermal cycling under silicone oil, another iteration with heating rate of 50 °C/s was performed, which appeared to match the initial 50 °C/s run, thereby confirming the role of silicone oil in protecting the sample from organic loss (Figure S7).<sup>5</sup> After one more iteration of melting at 250 °C/s, the material is cooled (2500 °C/s) and then crystallized (heating at 250 °C/s to 150 °C from -95 °C) before bringing it back to the room temperature for optical microscopy.

Calculation of sample mass: The mass of the S(1-2)NPB single crystal sample (166 ng) is determined by dividing the enthalpy of melting (6.24  $\mu$ J) obtained from the first iteration of the flash-DSC heating cycle in Figure 4a by the standard  $\Delta H_m$  value of 37.6 J/g obtained from the conventional DSC (Figure 2a). Also, assuming a hemispherical model of the blob with an average diameter of 65 micron (Figure 4b) and a density of 2.091 g/cm<sup>3</sup> (see Table S1 below), the approximate mass of the sample is calculated to be 150 ng, in qualitative agreement with the value from DSC comparisons.

#### 10. Optical microscopy:

The conventional and polarized optical microscopy of the crystallized S(1-2)NPB sample on the flash-DSC UFS-1 chip is carried out using Nikon Eclipse LV100N POL.

**Table S1.** Crystallographic and structural refinement data for S(1-2)NPB.

Empirical formula	C <sub>24</sub> H <sub>28</sub> Br <sub>4</sub> N <sub>2</sub> Pb
Formula weight	871.31
Temperature/K	297.51(19)
Crystal system	Monoclinic
Space group	<i>P</i> 2 <sub>1</sub>
<i>a</i> /Å	8.78233(15)
<i>b</i> /Å	7.84536(11)
<i>c</i> /Å	20.3617(4)
$\alpha$ /°	90
$\beta$ /°	99.4551(17)
$\gamma$ /°	90
Volume/Å <sup>3</sup>	1383.87(4)
<i>Z</i>	2
$\rho_{\text{calc}}$ / g/cm <sup>3</sup>	2.091
$\mu$ /mm <sup>-1</sup>	11.884
F(000)	816.0
Radiation	MoK $\alpha$ ( $\lambda$ = 0.71073)
2 $\Theta$ range for data collection/°	4.702 to 61.326
Reflections collected	24592
Independent reflections	7022 [ <i>R</i> <sub>int</sub> = 0.0237, <i>R</i> <sub>sigma</sub> = 0.0212]
Data/restraints/ parameters	7022/1/284
Goodness-of-fit on F <sup>2</sup>	1.021
Final R indexes [ <i>I</i> ≥ 2 $\sigma$ ( <i>I</i> )]	<i>R</i> <sub>1</sub> = 0.0200, <i>wR</i> <sub>2</sub> = 0.0444
Final R indexes [all data]	<i>R</i> <sub>1</sub> = 0.0252, <i>wR</i> <sub>2</sub> = 0.0455
Largest diff. peak/hole / e Å <sup>-3</sup>	0.82/-0.51
Flack parameter	-0.025(3)

**Table S2.** Summary of the NMR peak integration (taken from Figure S1) associated with S(1-2)NEA cation with respect to the peak of tetramethylsilane (TMS) as the internal reference.\*

Chemical shift (ppm)	Pristine S(1-2)NPB	After 1 cycle	After 3 cycles
8.17	2.9437	2.7103	1.9547
8.02	1.7819	1.6929	1.4495
7.97	1.7124	1.7462	1.4790
7.65	0.8669	0.8439	0.7203
7.41	1.0660	1.0844	0.8252
7.40	1.6926	1.6465	1.4105
1.60	2.7685	2.7825	2.4403

\*To quantify and compare the loss of S(1-2)NEA cation, the peaks at approximately 8.17, 8.02, 7.97, 7.65, 7.41, 7.40, and 1.60 ppm associated with S(1-2)NEA are integrated with respect to the peak of tetramethylsilane (TMS) as the internal reference. As the crystals underwent more thermal cycles, the overall decrease of the integration value of each peak represents the loss of a larger amount of S(1-2)NEA cation. Accounting for the number of hydrogens that each peak represents leads to the quantified average cation loss value of  $4 \pm 2\%$  for the crystals after one thermal cycle and  $19 \pm 7\%$  for the crystals after three thermal cycles.

**Table S3.** Table of FWHM values (obtained using X-pert data viewer program)<sup>6</sup> for the primary (002) XRD peaks of the S(1-2)NPB samples prepared under different conditions (See Figure 3 and Figure S2). The label “w/ Kapton” indicates that an overlying sheet of Kapton was present during the X-ray analysis (see “Melt processing of films” under Methods for details).

S(1-2)NPB sample	(002) peak position (°)	FWHM (°)
Powdered crystals (w/o Kapton)	4.409	0.061
Melt-quenched film (w/ Kapton)	4.280	0.086
Annealed film (w/ Kapton)	4.413	0.058
Annealed film (w/o Kapton)	4.406	0.052

**Table S4.** Glass formation ratio during preliminary testing of vitrification for S(1-2)NPB melt at a cooling rate of 250 °C/s (derived from taking the ratio of area under the cold crystallization peaks and area under the melting peak during heating runs. The curves are shown in Figure 4a). The samples were not heated after the 3<sup>rd</sup> cooling cycle; thus the glass formation ratio cannot be calculated in the final cycle.

	Melt crystallization enthalpy (μJ)	Cold crystallization enthalpy (μJ)	Melting enthalpy (μJ)	Glass formation ratio
1 <sup>st</sup> cycle	2.53	1.47	4.94	30.0 %
2 <sup>nd</sup> cycle	2.44	1.55	4.70	32.9 %
3 <sup>rd</sup> cycle	2.40	---	---	---

**Table S5.** Glass formation ratio for S(1-2)NPB vitrification at various cooling rates (derived from taking the ratio of area under the cold crystallization peaks and area under the melting peak during heating runs. The curves are shown in Figure 5b). Due to the convolution of the melt crystallization peak and the glass transition regime, the area under the melt crystallization peak couldn't be calculated for cooling rates  $\geq 1000$  °C/s.

	Melt crystallization enthalpy (μJ)	Cold crystallization enthalpy (μJ)	Melting enthalpy (μJ)	Glass formation ratio
After 250 °C/s cooling	2.04	1.53	4.19	36.5 %
After 500 °C/s cooling	0.61	2.95	3.93	75.1 %
After 1000 °C/s cooling	--	3.35	3.91	85.7 %
After 2500 °C/s cooling	--	3.71	3.90	95.1 %
After 5000 °C/s cooling	--	3.73	3.89	95.9 %

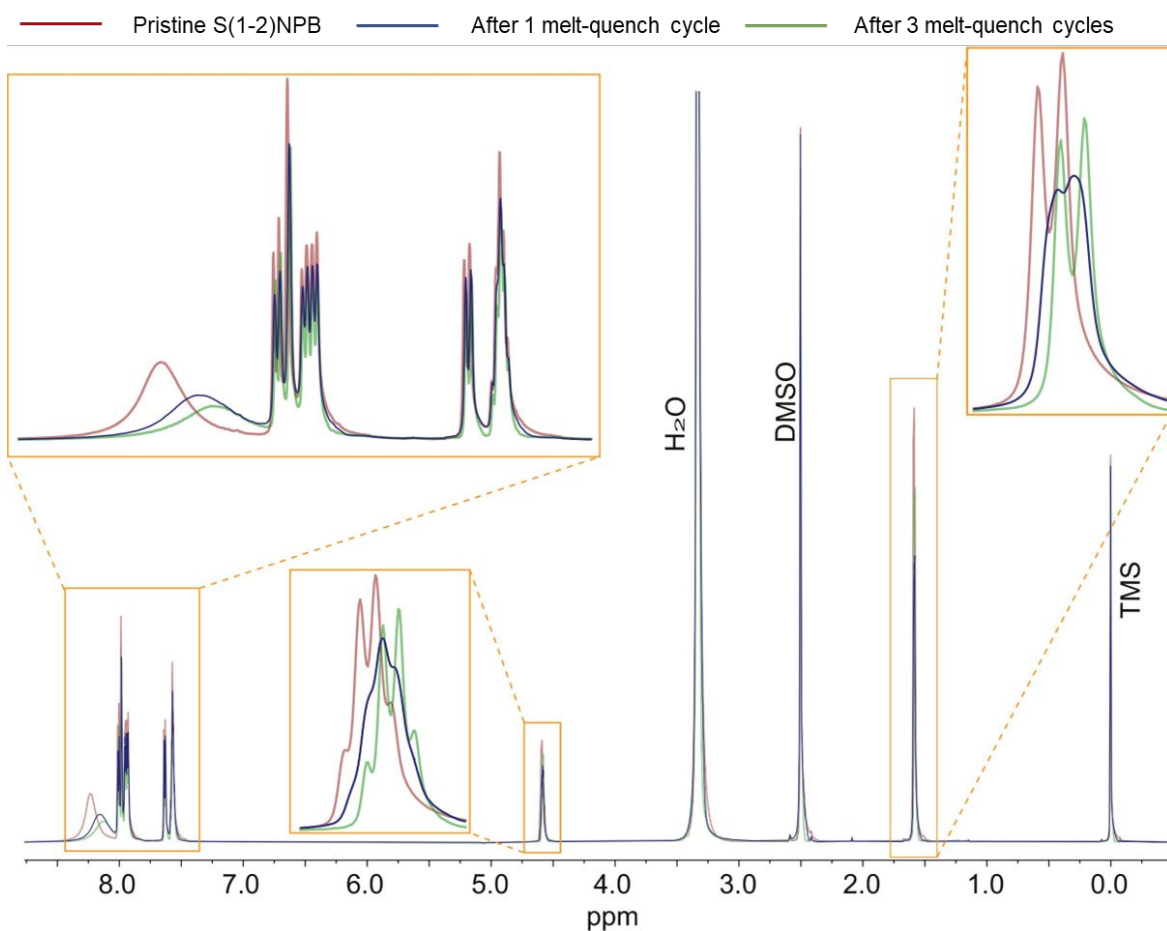


**Figure S1.**  $^1\text{H}$  NMR spectra of the pristine  $S(1-2)\text{NPB}$  crystals,  $S(1-2)\text{NPB}$  crystals that underwent one cycle of melt-quenching, and  $S(1-2)\text{NPB}$  crystals that underwent three cycles of melt-quenching. Owing to the thermal cycles, the  $S(1-2)\text{NEA}$  molecules undergo degradation, leading to less uniform chemical structures and many local structures with different thermal/conformational motions. As a result, the NMR peaks are broadening and shifting to different chemical shift values. The peak shift toward lower ppm (upfield shifts) could be due to the breaking of functional groups during degradation and the associated changes of the electron density around certain atoms. The reduction in area under the peaks, however, reveals the loss of organic molecules, with the corresponding areas under the NMR peaks provided in Table S2, which are utilized for calculating the decomposition percentage during thermal cycling.

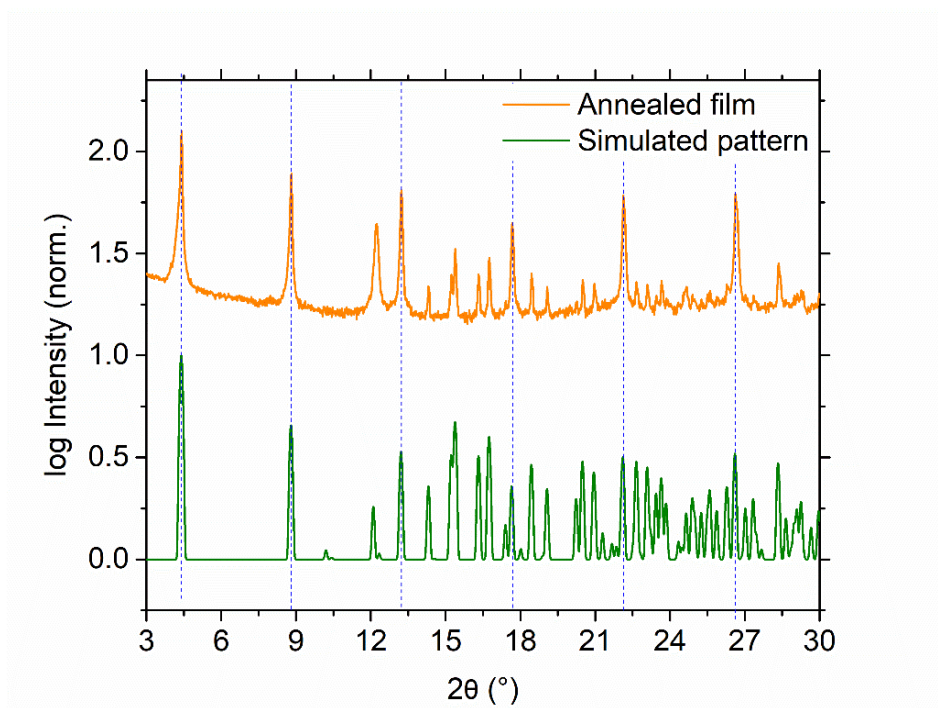


**Figure S2.** The normalized and logarithmic XRD pattern of the annealed S(1-2)NPB film, along with the simulated S(1-2)NPB pattern, demonstrates the phase purity of the deposited film, which exhibits multiple, but predominantly preferred (00l) orientations. The (00l) family of crystalline peaks are shown by vertical dotted blue lines as a guide to the eyes. The relatively broad peak at  $2\theta$  of  $\sim 12^\circ$  in the annealed film likely also contains a contribution from  $\text{PbBr}_2$  due to the high temperature processing and prospective sample degradation.<sup>7, 8</sup> The annealed film diffraction pattern is related to the pattern shown in Figure 3 albeit after removing the Kapton overlayer. The vertical axis is only for representation of scale, i.e., the curves are vertically offset for clarity.

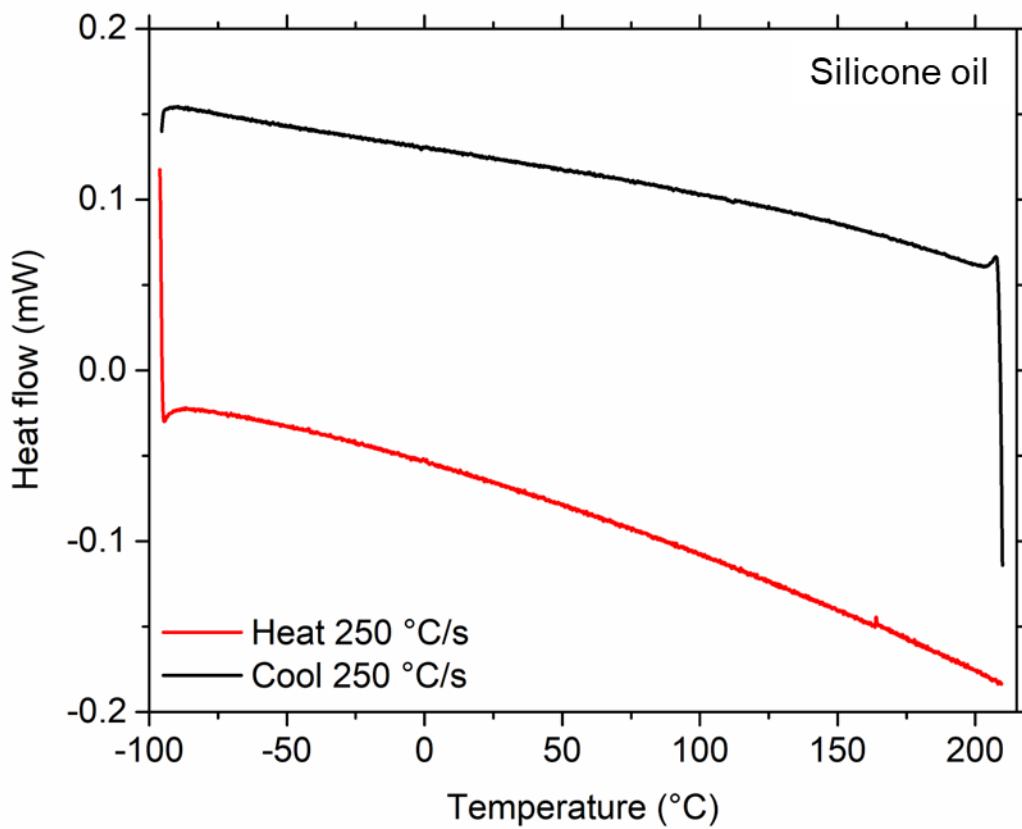


**Figure S3.** Flash-DSC curves obtained on heating and cooling silicone oil, which reveals no identifiable feature in the temperature region of interest.

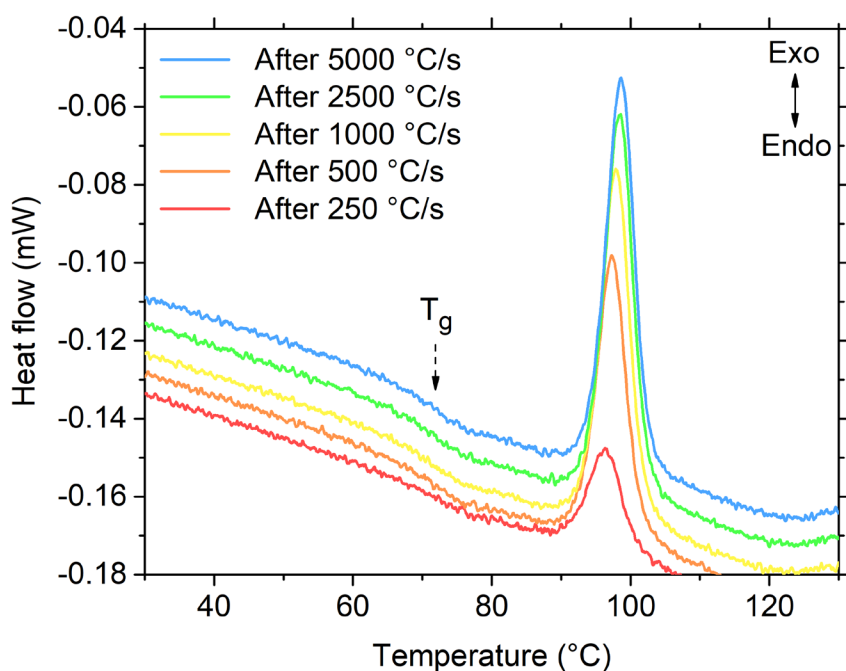


**Figure S4.** A closeup look at the glass transition regime for S(1-2)NPB obtained from enlarging Figure 5b. The curves are obtained at various heating rates. The vertical axis is only for representation of scale of magnitude, i.e., the curves are vertically offset for clarity.

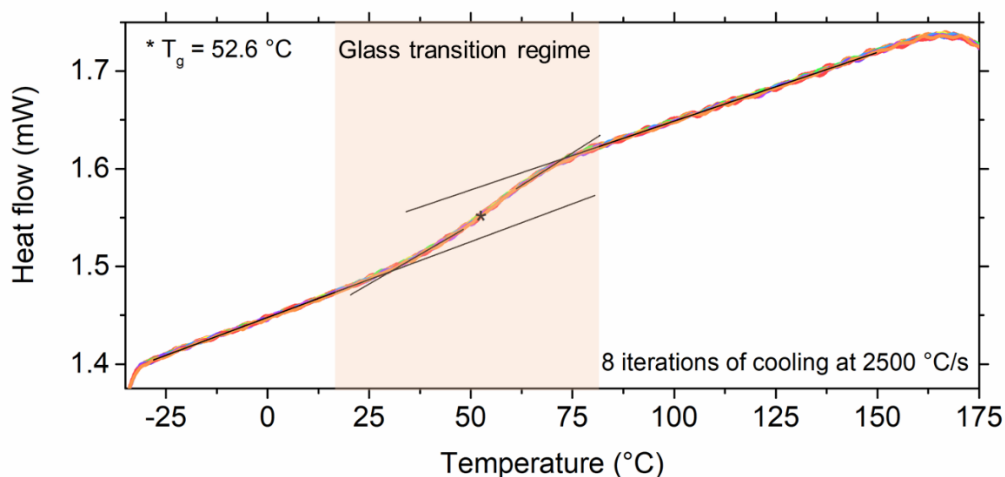


**Figure S5.** Flash-DSC cooling curves obtained during the kinetic study (Figure 6a) shows reproducible behavior over multiple iterations. A glass transition ( $T_g$ ) region is observed on cooling the melt at CCR (2500 °C/s).  $T_g = 52.6$  °C is obtained using the mid-point height technique (see Methods). There are eight cooling curves in the plot, and they all fall on top of each other.

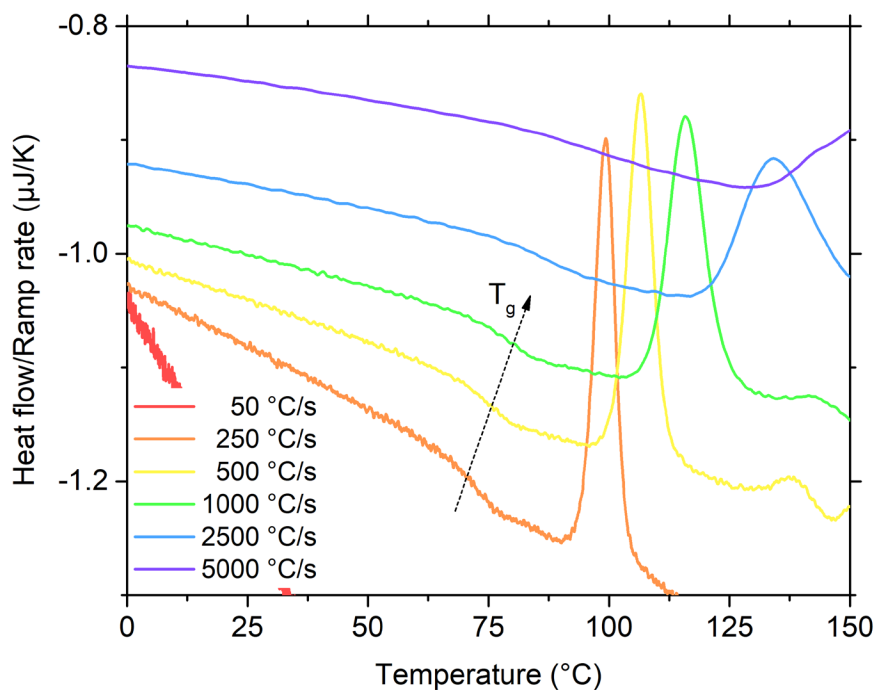


**Figure S6.** Normalized heating curves (with ramp rate) of *S(1-2)NPB* obtained at various heating rates after the glass formation step (melt quenching at CCR, See Figure S5). The shift in the glass transition temperature ( $T_g$ , shown by dotted arrow) on increasing heating rate shows the kinetic nature of the glass transition. The vertical axis is only for representation of scale of magnitude, i.e., the curves are vertically offset for clarity.

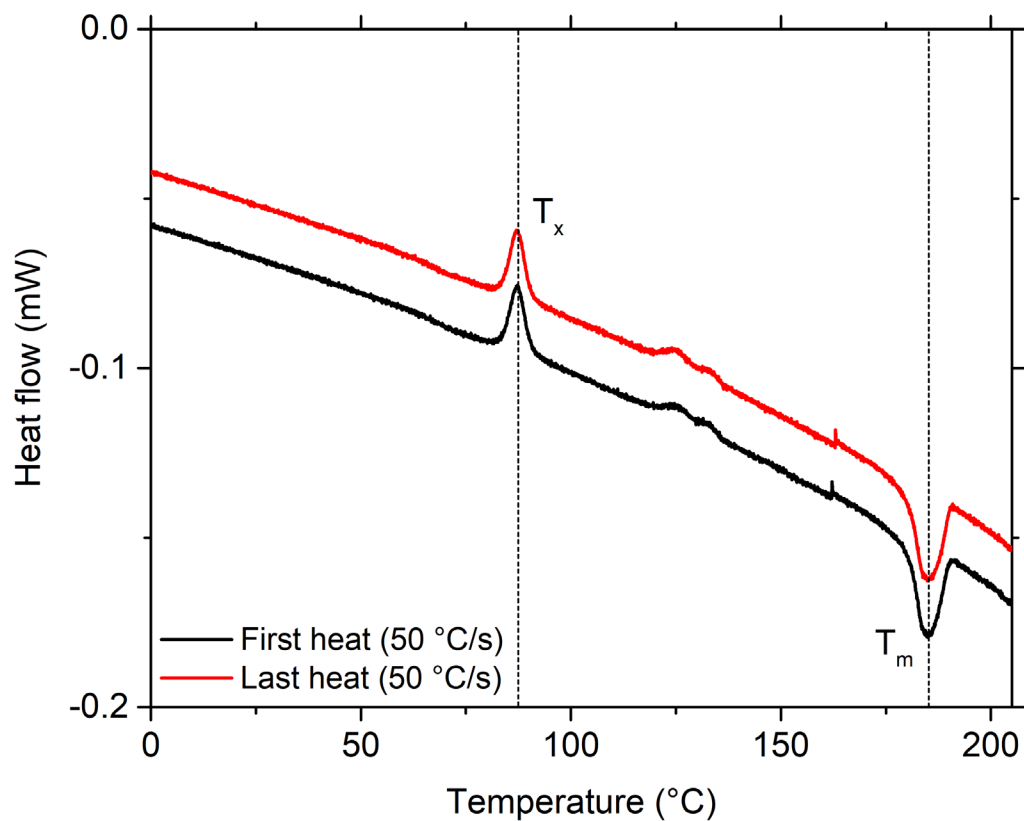


**Figure S7.** The first and the last heating measurement from the kinetic study (see Figure 6a) show similar crystallization and melting peak positions, revealing the robust nature of the measurement under silicone oil to circumvent organic loss. The vertical axis is only for representation of scale of magnitude, i.e., the curves are vertically offset for clarity.

## **Supplementary Section S1: Organic-inorganic H-bonding analysis**

For evaluating and comparing the organic-inorganic H-bonding strength between S(1-1)NPB and S(1-2)NPB, we developed a new supplementary methodology that quantitatively compiles and contrasts the positioning of N atoms in relation to the inorganic lattice, which serves as a means to assess the strength of organic-inorganic H-bonding interactions. As established in previous publications, the ammonium “penetration value” has served as a conventional parameter signifying the distance between the organic cation and the inorganic lattice.<sup>1</sup> Through our independent SC-XRD structural investigation, we have determined an average penetration of the ammonium group, quantified as the distance between the nitrogen (N) atom and the plane of axial bromine (Br) atoms, to be 0.26 Å for S(1-2)NPB and 0.17 Å for S(1-1)NPB (Table S6), which corroborates the outcomes documented by Moon *et al.*<sup>1</sup> A larger penetration of the ammonium group leads to closer distances between N atoms and equatorial Br atoms, potentially strengthening the H-bonding interactions with the corresponding equatorial Br atoms. However, this increased penetration can also lead to an expanded distance between N atoms and axial Br atoms.

To clarify the relative positions of the N atoms and the corresponding distances to the equatorial and axial Br atoms, we measured the distances between the N atoms and the adjacent Pb and Br atoms within the puckered square pattern formed by four interconnected distorted PbBr<sub>6</sub> octahedra (Figure 7a and Table S7 and Table S8). The N – Pb/Br distances are further illustrated and visualized by the radar chart (Figure 7b), revealing that the ammonium groups of S(1-1)NEA and S(1-2)NEA cations both adopt two types of positions (cation A and B, respectively). The positions of each type of ammonium group remain relatively consistent between S(1-1)NEA and S(1-2)NEA. However, by calculating the difference in N – Pb/Br distances between S(1-1)NEA and S(1-2)NEA cations, we can observe overall shorter N – Pb/Br distances of S(1-2)NEA cation B than for S(1-1)NEA cation B (Figure S8), suggesting that the S(1-2)NEA cation B is positioned in closer proximity to the inorganic lattice and may therefore potentially exhibit stronger H-bonding interactions. The N – Pb/Br distance differences are also calculated for S(1-1)NEA and S(1-2)NEA cation A (Figure S8); however, the results for this cation do not indicate a clear difference regarding the relative proximity or distance of the N atom to the inorganic lattice. The calculated larger penetration of the N atom of S(1-2)NEA cation B coincides with the corresponding shorter N – Pb/Br distances. Similarly, the comparable penetration of the N atom in cation A between S(1-1)NEA and S(1-2)NEA corresponds to the similar degree of N – Pb/Br distances. The observation of the stronger H-bonding interactions for S(1-2)NPB cation B (Figure S9 and Table S9) aligns with the closer proximity of S(1-2)NEA cation B to the inorganic lattice. It is noted that the H-bonding lengths (Table S9) are consistent with the values determined by Moon *et al.*<sup>1</sup> However, we additionally provide the H-bonding angles in this work. In the context of an unaltered donor (H<sub>2</sub>N-H) and acceptor (Br) combination, the strength of a H-bond is intricately linked to both bond length and angle. A shorter bond length and a larger bond angle (approaching 180°) typically indicate stronger H-bonding.

**Table S6.** Summary of ammonium group penetration in the inorganic layer of S(1-1)NPB and S(1-2)NPB. The obtained data for S(1-1)NPB is derived from our previously published work.<sup>9</sup>

		S(1-1)NPB	S(1-2)NPB
Penetration	N1 (Cation A)	0.12/0.24 Å	0.07/0.25 Å
	N2 (Cation B)	0.09/0.21 Å	0.27/0.44 Å
	N (Average)	0.17 Å	0.26 Å

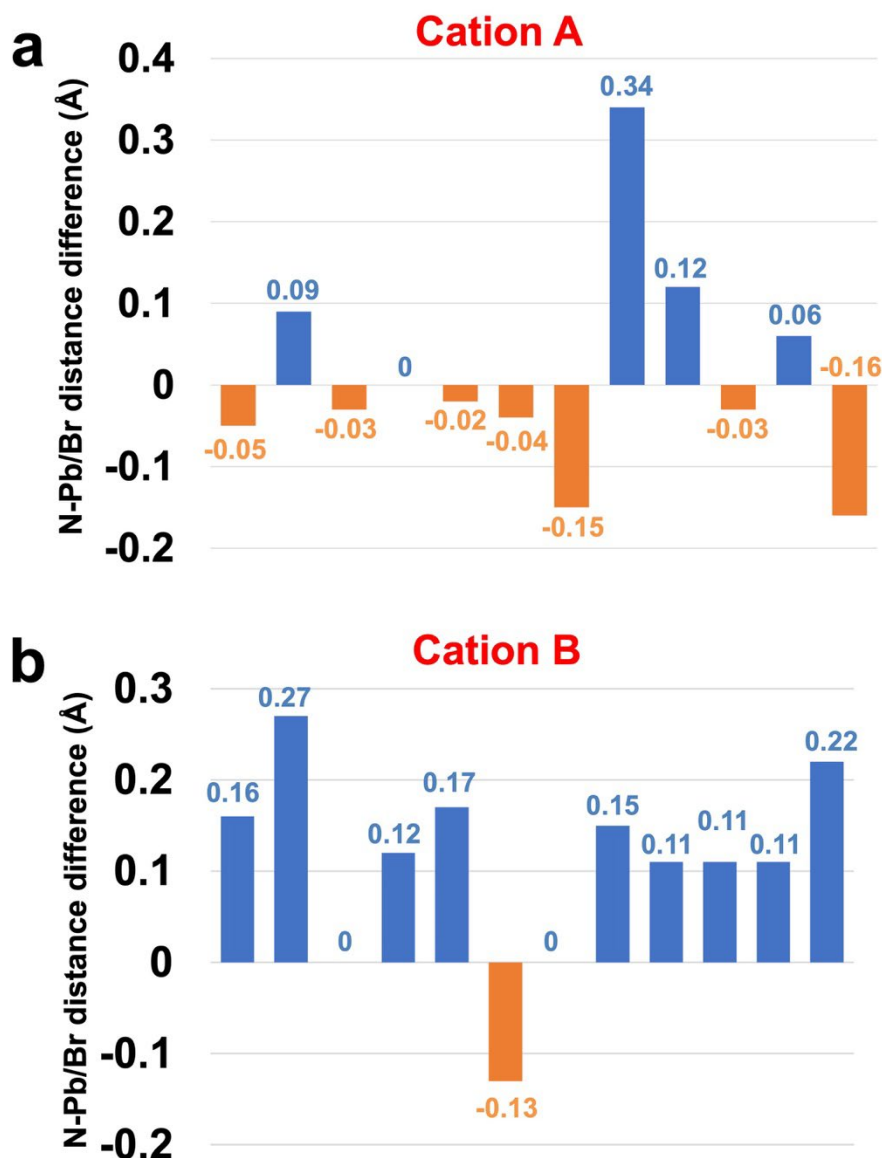


**Figure S8.** The calculated difference values in  $N - Pb/Br$  distances of (a) cation A between  $S(1-1)NEA$  and  $S(1-2)NEA$  cations, and (b) cation B between  $S(1-1)NEA$  and  $S(1-2)NEA$  cations. Different  $N - Pb$  and  $N - Br$  distances (as listed in Table S7) are distributed and plotted along the x-axis. Positive values are labeled with blue and negative values are labeled with orange. In panel b, the columns typically appear as blue, indicating that the  $N - Pb/Br$  distances for cation B in  $S(1-2)NPB$  are generally shorter relative to  $S(1-1)NPB$ . The obtained data for  $S(1-1)NPB$  is derived from a previously published work.<sup>9</sup>

**Table S7.** List of N – Pb/Br distances for the S(1-1)NPB cations labeled A and B (See Figure 7). The obtained data for S(1-1)NPB is derived from our previously published work.<sup>9</sup>

Cation A	N-Pb/Br distance (Å)	Cation B	N-Pb/Br distance (Å)
N (1) – Pb (1)	4.49	N (2) – Pb (1)	4.50
N (1) – Pb (1)	5.95	N (2) – Pb (1)	5.46
N (1) – Pb (1)	4.83	N (2) – Pb (1)	4.42
N (1) – Pb (1)	4.94	N (2) – Pb (1)	6.01
N (1) – Br (1)	3.37	N (2) – Br (1)	3.57
N (1) – Br (1)	5.39	N (2) – Br (1)	4.66
N (1) – Br (2)	3.47	N (2) – Br (2)	3.33
N (1) – Br (2)	4.92	N (2) – Br (2)	5.85
N (1) – Br (3)	3.76	N (2) – Br (3)	3.60
N (1) – Br (3)	5.43	N (2) – Br (3)	3.82
N (1) – Br (4)	3.49	N (2) – Br (4)	3.87
N (1) – Br (4)	3.86	N (2) – Br (4)	5.48

**Table S8.** List of N – Pb/Br distances for the S(1-2)NPB cations labeled A and B (See Figure 7).

Cation A	N-Pb/Br distance (Å)	Cation B	N-Pb/Br distance (Å)
N (1) – Pb (1)	4.54	N (2) – Pb (1)	4.34
N (1) – Pb (1)	5.86	N (2) – Pb (1)	5.19
N (1) – Pb (1)	4.86	N (2) – Pb (1)	4.42
N (1) – Pb (1)	4.94	N (2) – Pb (1)	5.89
N (1) – Br (1)	3.39	N (2) – Br (1)	3.40
N (1) – Br (1)	5.43	N (2) – Br (1)	4.79
N (1) – Br (2)	3.62	N (2) – Br (2)	3.33
N (1) – Br (2)	4.58	N (2) – Br (2)	5.70
N (1) – Br (3)	3.64	N (2) – Br (3)	3.49
N (1) – Br (3)	5.46	N (2) – Br (3)	3.71
N (1) – Br (4)	3.43	N (2) – Br (4)	3.76
N (1) – Br (4)	4.02	N (2) – Br (4)	5.26

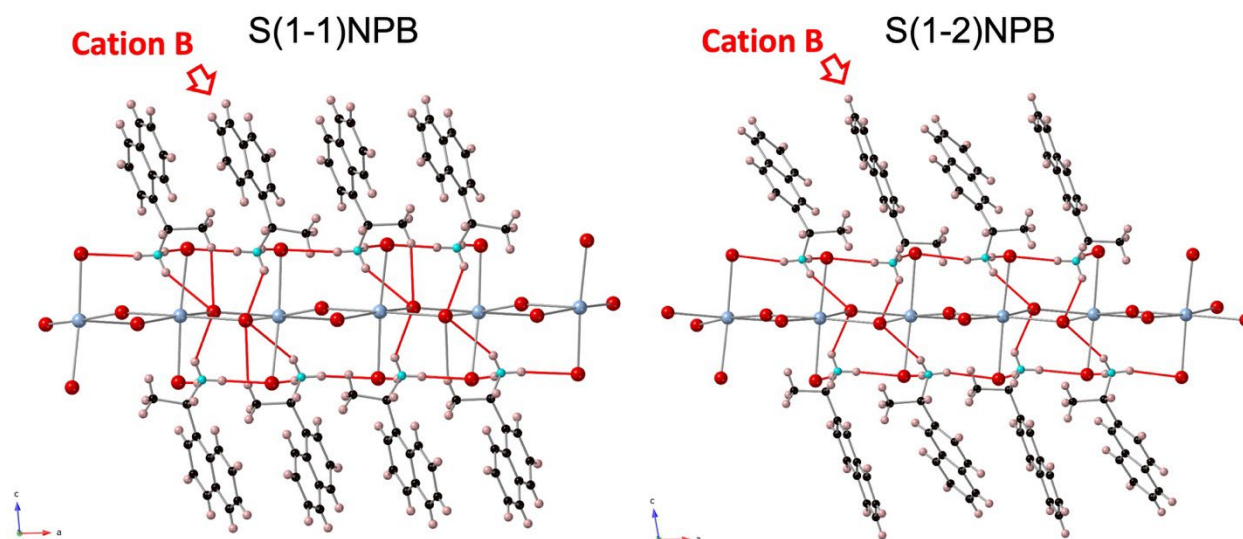


**Figure S9.** The hydrogen-bonding interactions between the axial and equatorial Br atoms and  $NEA^+$  cations in  $S(1-1)NPB$  and  $S(1-2)NPB$ . The type B cations are labeled. Blue, red, black, turquoise, and beige spheres denote Pb, Br, C, N, and H atoms, respectively. The obtained data for  $S(1-1)NPB$  is derived from a previously published work.<sup>9</sup>

**Table S9.** List of hydrogen-bonding lengths and angles for  $S(1-1)NPB$  and  $S(1-2)NPB$  structures. The obtained data for  $S(1-1)NPB$  is derived from a previously published work.<sup>9</sup>

	S(1-1)NPB		S(1-2)NPB	
	Bond length (Å)	Angle (°)	Bond length (Å)	Angle (°)
Cation A	2.48	174.55	2.52	164.73
	2.59	171.90	2.73	177.94
	2.93	155.24	2.79	160.61
	2.85	158.15		
Cation B	2.69	169.00	2.52	169.38
	2.48	159.44	2.48	161.05
	2.88	138.34	2.81	133.90

## References:

1. J. Son, S. Ma, Y.-K. Jung, J. Tan, G. Jang, H. Lee, C. U. Lee, J. Lee, S. Moon, W. Jeong, A. Walsh and J. Moon, Unraveling chirality transfer mechanism by structural isomer-derived hydrogen bonding interaction in 2D chiral perovskite, *Nat. Commun.*, 2023, **14**, 3124.
2. V. Mathot, M. Pyda, T. Pijpers, G. V. Poel, E. Van de Kerkhof, S. Van Herwaarden, F. Van Herwaarden and A. Leenaers, The Flash DSC 1, a power compensation twin-type, chip-based fast scanning calorimeter (FSC): First findings on polymers, *Thermochim. Acta*, 2011, **522**, 36-45.
3. J. Schawe, Practical aspects of the Flash DSC 1: Sample preparation for measurements of polymers [https://www.mt.com/us/en/home/supportive\\_content/matchar\\_apps/MatChar\\_UC364.html](https://www.mt.com/us/en/home/supportive_content/matchar_apps/MatChar_UC364.html) (Accessed November 2023).
4. Flash Differential Scanning Calorimetry: [https://www.testunlimited.com/pdf/MT\\_DSC2\\_Datasheet.pdf](https://www.testunlimited.com/pdf/MT_DSC2_Datasheet.pdf) (Accessed November 2023).
5. A. Singh, Y. Kim, R. Henry, H. Ade and D. B. Mitzi, Study of Glass Formation and Crystallization Kinetics in a 2D Metal Halide Perovskite Using Ultrafast Calorimetry, *J. Am. Chem. Soc.*, 2023, **145**, 18623-18633.
6. X'pert Data Collector: <https://web.stanford.edu/group/glam/xlab/PhilipsLit/Data%20Collector%20QSG.pdf> (Accessed November 2023).
7. N. K. Kumawat, N. Jain, A. Dey, K. Narasimhan and D. Kabra, Quantitative correlation of perovskite film morphology to light emitting diodes efficiency parameters, *Adv. Funct. Mater.*, 2017, **27**, 1603219.
8. F. Chen, C. Xu, Q. Xu, Y. Zhu, F. Qin, W. Zhang, Z. Zhu, W. Liu and Z. Shi, Self-assembled growth of ultrastable CH<sub>3</sub>NH<sub>3</sub>PbBr<sub>3</sub> perovskite milliwires for photodetectors, *ACS Appl. Mater. Interfaces*, 2018, **10**, 25763-25769.
9. M. K. Jana, R. Song, H. Liu, D. R. Khanal, S. M. Janke, R. Zhao, C. Liu, Z. V. Vardeny, V. Blum and D. B. Mitzi, Organic-to-inorganic structural chirality transfer in a 2D hybrid perovskite and impact on Rashba-Dresselhaus spin-orbit coupling, *Nat. Commun.*, 2020, **11**, 4699.